

## Determination of collision mechanisms at low energies using four-vector correlations

P. G. Jambrina,  <sup>\*a</sup> J. F. E. Croft,  <sup>b</sup> N. Balakrishnan,  Hua Guo  <sup>d</sup> and F. J. Aoiz  <sup>e</sup>

Received 16th December 2023, Accepted 19th February 2024

DOI: 10.1039/d3fd00173c

In molecular dynamics, a fundamental question is how the outcome of a collision depends on the relative orientation of the collision partners before their interaction begins (the stereodynamics of the process). The preference for a particular orientation of the reactant complex is intimately related to the idea of a collision mechanism and the possibility of control, as revealed in recent experiments. Indeed, this preference holds not only for chemical reactions involving complex polyatomic molecules, but also for the simplest inelastic atom–diatom collisions at cold collision energies. In this work, we report how the outcome of rotationally inelastic collisions between two D<sub>2</sub> molecules can be controlled by changing the alignment of their internuclear axes under the same or different polarization vectors. Our results demonstrate that a higher degree of control can be achieved when two internuclear axes are aligned, especially when both molecules are relaxed in the collision. The possibility of control extends to very low energies, even to the ultracold regime, when no control could be achieved just by the alignment of the internuclear axis of one of the colliding partners.

### 1 Introduction

The outcome of a bimolecular collision is determined by the chemical nature of the colliding partners, their internal states, the relative translational (collision) energy, as well as their relative orientation as they approach each other (the stereodynamics of the process). This statement holds for complex chemical

<sup>a</sup>Departamento de Química Física, Universidad de Salamanca, Salamanca 37008, Spain. E-mail: pjambrina@usal.es

<sup>b</sup>Department of Chemistry, Durham University, Durham, DH1 3LE, UK. E-mail: james.f.croft@durham.ac.uk

<sup>c</sup>Department of Chemistry and Biochemistry, University of Nevada, Las Vegas, Nevada 89154, USA. E-mail: naduvala@unlv.nevada.edu

<sup>d</sup>Department of Chemistry and Chemical Biology, University of New Mexico, Albuquerque, New Mexico 87131, USA. E-mail: hgwo@unm.edu

<sup>e</sup>Departamento de Química Física, Universidad Complutense, Madrid 28040, Spain. E-mail: aoiz@quim.ucm.es



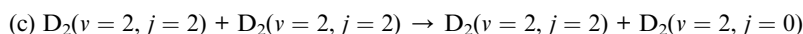
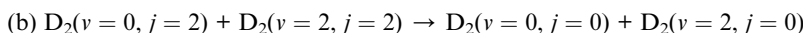
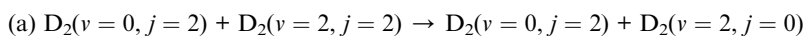
reactions, where the dependence of the reactivity on the stereodynamics of the reaction is intimately related to the idea of a reaction mechanism and can be traced back to the anisotropy (direction) of the chemical bonds that are broken or formed,<sup>1–6</sup> and also applies to simpler reactions between an atom and a diatomic molecule.<sup>7–11</sup> On top of this, stereodynamics determines the properties of the products formed during chemical reactions, such as for example the propensity for given  $\Lambda$ -doublet states experimentally found in the  $\text{O}({}^3\text{P}) + \text{D}_2$  reaction.<sup>12–15</sup>

For inelastic collisions no bonds are formed or broken, and the products of the collision differ from the reactants just in the rotational and/or vibrational energy levels, so it is not that obvious how (or if) the outcome of the collision will be modified by the stereodynamics of the collision. However, experiments have consistently found that the outcome of inelastic collisions is also strongly dependent on the relative orientation of the molecules before the collision (see for example ref. 16–30). Recent advances combining Stark-induced adiabatic Raman passage (SARP) with a co-expansion beam have made it possible to study the stereodynamics of inelastic collisions at cold energies (below 1 K).<sup>25–30</sup> At these energies, scattering is dominated by quantum resonances, and calculations have proved that by selecting a suitable relative orientation of the reactants it is possible to modify (control) to a significant extent the integral (ICS) and differential cross sections (DCS).<sup>31–42</sup>

The stereodynamics of a process can be quantified in terms of correlations between the vector properties of the collision system.<sup>43–51</sup> The simplest, the differential cross section, quantifies the correlation the initial ( $\mathbf{k}$ ) and final ( $\mathbf{k}'$ ) relative velocities of the collision partners. Three vector correlations involving the direction of the rotational angular momentum of one of the colliding partners ( $\mathbf{j}_A$ ) as well as  $\mathbf{k}$  and final  $\mathbf{k}'$  provides information about how the collision outcome will depend on the direction  $\mathbf{j}_A$  with respect to  $\mathbf{k}$ . Analysis of this vector correlation is necessary to account for most of the experiments cited above, and to describe the collision mechanism for reactive or inelastic collisions between an atom and a diatomic molecule. Recent breakthrough experiments<sup>20,30</sup> have been able to measure 4-vector correlations involving  $\mathbf{k}$ ,  $\mathbf{k}'$ ,  $\mathbf{j}_A$ , and either the direction of the angular momentum after the collision  $\mathbf{j}_A^{'}<sup>20</sup>$  or the direction of the angular momentum of the other partner ( $\mathbf{j}_B$ ).<sup>30</sup> The latter measurements were successfully simulated from first principles, combining quantum scattering calculations on an accurate potential energy surface and a formalism that describes up to four vector correlations.<sup>41</sup>

In this work, we go beyond the simulation of the experimental angular distributions and study how the collision mechanism for the inelastic collisions between two diatomic molecules can be determined through the analysis of the  $\mathbf{k}$ – $\mathbf{j}_A$ – $\mathbf{j}_B$ – $\mathbf{k}'$  4-vector correlation, even for situations in which the polarisation of the two incoming molecules is different. Crossed molecular beam experiments in which the two collision partners are independently polarised, for instance using SARP schemes for the two beams, are conceivable. Of course, performing such experiments at cold energies entails additional difficulties. However, the successes achieved over the last decade with merged beams<sup>52–55</sup> or Stark<sup>56–58</sup> and Zeeman<sup>59</sup> decelerators suggest that such experiments may be feasible in the near future. The system that we will study is the  $\text{D}_2(v, j = 2) + \text{D}_2(v, j = 2)$  at cold energies, as this was the system studied in ref. 30. In particular, we will focus on quantum effects such as resonances, their influence on the reaction mechanism, and how they are modified by the alignment and orientation of the collision complex. We will analyze three different scenarios:





In cases (a) and (c) only one of the  $D_2$  molecules is relaxed from  $j = 2$  to  $j = 0$ , with the difference that in case (a) we have two “distinguishable” molecules, while in case (c) we have two identical  $D_2(v = 2)$  molecules. Case (b) corresponds to a situation in which both molecules are relaxed during the collision. Cases (a) and (b) involve the rotational excitation of one of the partners (pure rotational pumping), whilst case (c) involves the vibrational excitation of the two partners as in a recent work using SARP.<sup>30</sup>

The paper is organized as follows. The equations needed to calculate the 4-vector correlations and the details of the scattering calculations are shown in Section 2. Results for the three different cases are discussed in Section 3, while the main conclusions are summarized in Section 4.

## 2 Methods

### 2.1 Scattering calculations

Full dimension QM scattering calculations were performed using the time-independent close-coupling formalism and a modified version of the TwoBC code<sup>60</sup> on the recent PES of Zuo *et al.*<sup>61</sup> In these calculations, the two  $D_2$  molecules were treated as indistinguishable molecules, following the convention of Huo and Green.<sup>62</sup> In the calculations, the close coupling equations were propagated using a log-derivative method from 3 to  $103a_0$  with a step size of  $0.05a_0$ . Calculations were carried out for each parity and exchange permutation symmetry, up to a maximum value of the total angular momentum  $J_{\max} = 16$ .<sup>42</sup>

The asymptotic scattering amplitude was obtained in the orbital angular momentum representation. However, for our purposes here it is more convenient to convert the scattering amplitudes into the helicity or body-fixed representation. The transformation of the  $T$ -matrix ( $T = I - S$ ) from the space-fixed (SF) to the helicity representation is given by<sup>63</sup>

$$T_{j_{AB}, m_A, m_B, m_{AB} \rightarrow j'_{AB}, m'_A, m'_B, m'_{AB}}^{J, \pm} = \sum_{\ell, \ell'} i^{\ell - \ell'} \frac{[(2\ell + 1)(2\ell' + 1)]^{1/2}}{2J + 1} \times \left\langle \ell' 0 j' m'_{AB} \left| J m'_{AB} \right. \right\rangle \langle \ell 0 j m_{AB} | J m_{AB} \rangle \langle j_A m_A j_B m_B | j_{AB} m_{AB} \rangle \times \left\langle j'_A m'_A j'_B m'_B \left| j'_{AB} m'_{AB} \right. \right\rangle \times T_{j'_{AB}, \ell', j_{AB}, \ell}^{J, \pm}, \quad (1)$$

where  $\langle \dots | \dots \rangle$  denotes a Clebsch-Gordan coefficient,  $J$  is the total angular momentum quantum number,  $\ell$  ( $\ell'$ ) is the initial (final) orbital angular momentum, and  $j_A$ ,  $j_B$ ,  $j'_A$  and  $j'_B$  are the initial and final rotational angular momentum quantum numbers of A and B molecules. The quantum numbers  $m_{A/B}$  and  $m'_{A/B}$  are the projections of  $j_{A/B}$  and  $j'_{A/B}$  onto the initial relative velocity vector and  $j_{AB} = j_A + j_B$  and  $j'_{AB} = j'_A + j'_B$ . The indices that denote the asymptotic



channel (initial and final rovibrational states) have been omitted for clarity. In eqn (1) the  $\pm$  index denotes the exchange permutation symmetry index of the molecules, and the last two Clebsch–Gordan coefficients guarantee that  $m_{AB} = m_A + m_B$  and  $m'_{AB} = m'_A + m'_B$ , so in what follows  $m_{AB}$  and  $m'_{AB}$  will be omitted for the sake of simplicity. From the  $S$  matrix in the helicity representation, the scattering amplitude can be calculated as:

$$F_{m'_A m'_B m_A m_B}^{\pm}(\theta) = \frac{\sqrt{(1 + \delta_{v_A v_B} \delta_{j_A j_B})(1 + \delta_{v'_A v'_B} \delta_{j'_A j'_B})}}{2ik} \times \sum_J \sum_{j_{AB} j'_{AB}} (2J + 1) d_{m'_{AB}, m_{AB}}^J(\theta) S_{j'_{AB} m'_A m'_B j_{AB} m_A m_B}^{J, \pm}, \quad (2)$$

where  $k = (2\mu E_{\text{coll}}/\hbar)^{1/2}$  is the initial relative wave vector,  $\mu$  the reduced mass, and  $E_{\text{coll}}$  the collision energy, and  $d_{m'_{AB}, m_{AB}}^J(\theta)$  is an element of the Wigner reduced rotation matrix. The  $\sqrt{(1 + \delta_{v_A v_B} \delta_{j_A j_B})(1 + \delta_{v'_A v'_B} \delta_{j'_A j'_B})}$  factor only applies for inelastic scattering between indistinguishable molecules.<sup>64,65</sup>

The exchange-permutation symmetrized differential cross section (DCS) is given in terms of the corresponding scattering amplitudes:

$$\frac{d\sigma^{\pm}}{d\Omega}(\theta) = \frac{1}{(2j_A + 1)(2j_B + 1)} \times \sum_{m'_A m'_B m_A m_B} F_{m'_A m'_B m_A m_B}^{\pm}(\theta) \left[ F_{m'_A m'_B m_A m_B}^{\pm}(\theta) \right]^*, \quad (3)$$

and the statistically weighted DCS is obtained as:

$$\frac{d\sigma}{d\Omega}(\theta) = w^+ \frac{d\sigma^+}{d\Omega}(\theta) + w^- \frac{d\sigma^-}{d\Omega}(\theta) \quad (4)$$

where the  $w^{\pm}$  coefficients are the statistical weights of nuclear spin states associated with the two exchange symmetries. For collisions between two *o*-D<sub>2</sub> ( $j$  = even) molecules:<sup>66</sup>

$$w^+ = \frac{21}{36}, \quad w^- = \frac{15}{36}. \quad (5)$$

## 2.2 4-Vector correlations

Miranda and Clary<sup>46,50</sup> and Balint-Kurti and Vasyutinskii<sup>51</sup> provided formalisms to calculate 4-vector correlations. The methodology presented here is an extension of the 3-vector correlations methodology used by Aoiz, Miranda and coworkers.<sup>47–49,67</sup> It is based on the distinction between “intrinsic” and “extrinsic” polarization moments. The extrinsic polarization moments describe and quantify the actual preparation of the incoming molecules in a hypothetical (or real) experiment; they depend on the properties of the experiment rather than on the collision dynamics. In the scattering frame, the extrinsic polarization parameters,  $a_q^{(k)}$ , are given by

$$a_q^{(k)} = C_{kq}(\beta, \alpha) A_0^{(k)} \quad (6)$$



where  $A_0^{(k)}$  are the extrinsic polarization parameters (PPs) in the laboratory frame, and  $C_{kq}$  are the modified spherical harmonics ( $C_{kq}(\theta, \phi) = [4\pi/(2k+1)]^{1/2} Y_{kq}(\theta, \phi)$ ), where  $Y_{kq}(\theta, \phi)$  are the spherical harmonics.  $\beta$  and  $\alpha$  are the polar and azimuthal angles that define the direction of the polarization vector in the scattering frame, and they rotate the extrinsic polarization parameters in the laboratory frame ( $A_0^{(k)}$ ) to the scattering frame ( $a_q^{(k)}$ ). The use of  $C_{kq}$  implies that the experimental preparation in the laboratory frame has cylindrical symmetry along the laboratory axis.<sup>49</sup> If we assume a hypothetical experiment in which one reactant is prepared in a pure  $|j_A m_A = 0\rangle$  state, where  $m_A$  denotes the magnetic quantum number with respect to a laboratory-fixed axis (the polarization vector of the Stokes and pump laser in the SARP experiment),  $A_0^{(k)} = \langle j_A 0, k | j_A 0 \rangle$ . The preparation of a  $|j = 2, m = 0\rangle$  state can be achieved, for example, by optical state preparation using the Stark-induced adiabatic Raman passage (SARP) method. Unless the preparation (polarization) of the two reactants is equivalent, different extrinsic polarization parameters are required for each of them. In the particular case in which one of them is unpolarized (unprepared) the only non-vanishing extrinsic polarization parameter for that reactant is  $A_0^{(0)} = 1$ .

The intrinsic polarization parameters (PDDCSs from Polarization Dependent Differential Cross Sections), in turn, do not depend on the experimental set-up but on the collision dynamics. They are intimately connected to the idea of collision mechanisms, with the difference that polarization parameters can be quantified. For the  $\mathbf{k} \cdot \mathbf{j}_A \cdot \mathbf{j}_B \cdot \mathbf{k}'$  four-vector correlation corresponding to the polarization of the two rotational angular momenta before the collision, the PDDCSs can be calculated in the uncoupled representation as:<sup>41</sup>

$$U_{q_A, q_B}^{(k_A, k_B), \pm}(\theta) = \frac{1}{(2j_A + 1)(2j_B + 1)} \times \sum_{m_A', m_B', m_A m_B} F_{m_A' m_B' m_A m_B}^{\pm}(\theta) \left[ F_{m_A' m_B' (m_A + q_A)(m_B + q_B)}^{\pm}(\theta) \right]^* \times \langle j_A m_A, k_A q_A | j_A (m_A + q_A) \rangle \langle j_B m_B, k_B q_B | j_B (m_B + q_B) \rangle. \quad (7)$$

where  $U_{q_A, q_B}^{(k_A, k_B), \pm}$  is the PDDCS with rank  $k_A \times k_B$  and components  $(q_A, q_B)$ . The possible values of  $k_A$ ,  $k_B$ ,  $q_A$ , and  $q_B$  are limited by the Clebsch–Gordan coefficients of eqn (7). Hence,

$$0 \leq k_A \leq 2j_A, 0 \leq k_B \leq 2j_B \quad (8)$$

$$-k_A \leq q_A \leq k_A, -k_B \leq q_B \leq k_B. \quad (9)$$

It should be noted that  $U_{0,0}^{0,0, \pm}(\theta)$  is nothing but the isotropic (no preparation) DCS, and that if either  $k_A$  or  $k_B$  are zero, we recover the expression for the three vector correlations PDDCSs corresponding to the polarization of  $\mathbf{j}_B$  and  $\mathbf{j}_A$ , respectively. An equation similar to (4) holds for the calculation of the unsymmetrized  $U_{q_A, q_B}^{(k_A, k_B)}$ . Similarly, for distinguishable particles, the  $U_{q_A, q_B}^{(k_A, k_B)}$  can be calculated straight from eqn (7).

Once the 4-vector correlations have been calculated, the observable DCS can be evaluated as:



$$d\sigma^\pm(\theta|\beta_1, \beta_2, \alpha_1, \alpha_2) = \sum_{k_A=0}^{2j_A} \sum_{q_A} \sum_{k_B=0}^{2j_B} \sum_{q_B} (2k_A + 1)(2k_B + 1) \\ \times \left[ U_{q_A, q_B}^{(k_A, k_B), \pm}(\theta) \right]^* a_{q_A}^{(k_A)} a_{q_B}^{(k_B)}, \quad (10)$$

where  $\beta_1$  ( $\beta_2$ ) and  $\alpha_1$  ( $\alpha_2$ ) are the polar and azimuthal angles that define the direction of the polarization vector of A (B) in an experiment where both molecules could be polarized independently. The dependence of the observable DCS on these angles is included implicitly in  $a_{q_A}^{(k_A)}$  and  $a_{q_B}^{(k_B)}$ , which can be calculated following eqn (6).

Similar to the PDDCSs corresponding to the three vector correlations, the  $U_{q_A, q_B}^{(k_A, k_B), \pm}$  defined in eqn (7) are complex numbers. If  $k_A + k_B$  is even, the  $U_{q_A, q_B}^{(k_A, k_B), \pm}$  only have a real part, while if  $k_A + k_B$  is odd, they are purely imaginary. Moreover, in the particular case of  $q_A = 0$  and  $q_B = 0$  the only non-vanishing  $U_{0,0}^{(k_A, k_B)}$  are those for which  $k_A + k_B$  is even.

To quantify the effect of reactants polarization on the integral cross section, it is necessary to calculate the polarization moments,  $U_{q_A, q_B}^{(k_A, k_B), \pm}$ , which are defined as:

$$u_{q_A, q_B}^{(k_A, k_B), \pm} = \int_{-1}^{+1} U_{q_A, q_B}^{(k_A, k_B), \pm}(\theta) d(\cos \theta). \quad (11)$$

Eqn (11) is general but requires the calculation of  $U_{q_A, q_B}^{(k_A, k_B), \pm}(\theta)$ . For the particular case of  $q_A = 0$  and  $q_B = 0$  the  $U_{q_A, q_B}^{(k_A, k_B), \pm}$  can also be calculated straight from the modulus of the scattering matrix elements, as:

$$u_{0,0}^{(k_A, k_B), \pm} = \frac{\pi}{k^2} (1 + \delta_{v_A v_B} \delta_{j_A j_B}) \left( 1 + \delta_{v'_A v'_B} \delta_{j'_A j'_B} \right) \frac{1}{(2j_A + 1)(2j_B + 1)} \\ \times \sum_{j_{AB} m_A, m_B} \sum_{j'_{AB} m'_A, m'_B} \sum_J (2J + 1) \left| S_{j'_{AB} m'_A, m'_B, j_{AB} m_A, m_B}^{J, \pm} \right|^2 \\ \times \langle j_A m_A, k_A | j_A m_A \rangle \langle j_B m_B, k_B | j_B m_B \rangle \quad (12)$$

where the  $(1 + \delta_{v_A v_B} \delta_{j_A j_B})(1 + \delta_{v'_A v'_B} \delta_{j'_A j'_B})$  applies only to inelastic scattering between indistinguishable molecules. Note that  $u_{0,0}^{(0,0), \pm}$  is the isotropic ICS.

The observable ICS, *i.e.* the ICS for an experiment in which the two molecules are polarized, can be calculated from the integration of the observable DCS (eqn (10)) over the azimuthal, and the scattering angle. The resulting expression is:

$$\sigma^\pm(\beta_1, \beta_2) = \sum_{k_A=0}^{2j_A} \sum_{k_B=0}^{2j_B} (2k_A + 1)(2k_B + 1) \\ \times \left[ u_{0,0}^{(k_A, k_B), \pm} \right]^* a_0^{(k_A)} a_0^{(k_B)}, \quad (13)$$

where the dependence over  $\alpha_1$  and  $\alpha_2$  as well as the moments with  $q_A \neq 0$  or  $q_B \neq 0$  have vanished due to the integration over the azimuthal angle and the properties of the modified spherical harmonics.

As just described, the intrinsic PDDCSs and PPs express how the DCS and ICS change with reactant polarization in absolute terms, as they are proportional to the isotropic DCS and ICS, respectively. Sometimes it is important to express them relative to the isotropic DCS or ICS so they can convey how important the

effect of the polarization is for those observables. The normalized PPs, denoted as  $s_{q_A, q_B}^{(k_A, k_B), \pm}$  can be calculated as:

$$s_{q_A, q_B}^{(k_A, k_B), \pm} = \frac{u_{q_A, q_B}^{(k_A, k_B), \pm}}{u_{0,0}^{(0,0)}}. \quad (14)$$

## 3 Results

### 3.1 $D_2(v = 0, j = 2) + D_2(v = 2, j = 2) \rightarrow D_2(v = 0, j = 2) + D_2(v = 2, j = 0)$

We begin with a discussion of  $D_2(v = 0, j = 2) + D_2(v = 2, j = 2) \rightarrow D_2(v = 0, j = 2) + D_2(v = 2, j = 0)$  collisions. The two molecules are treated as indistinguishable in the scattering calculations, but in the range of  $E_{\text{coll}}$  considered here we find that  $S_{j_{AB} m'_A, m'_B j_{AB} m_A m_B}^{J,+} \sim S_{j_{AB} m'_A, m'_B j_{AB} m_A m_B}^{J,-}$ , which indicates that the two collision partners are effectively distinguishable<sup>62</sup> (the probability of going from  $v = 2$  to  $v = 0$  and simultaneously from  $v = 0$  to  $v = 2$  is negligible). According to this, we can describe this process as the rotational quenching from  $D_2(v = 2, j = 2)$  to  $D_2(v = 2, j = 0)$  induced by a collision with a  $D_2(v = 0, j = 2)$  molecule that does not change its initial state.

Panel (a) of Fig. 1 shows the isotropic (no polarization) excitation function, *i.e.* the cross section as a function of  $E_{\text{coll}}$  in the 1 mK–100 K range. Along with the isotropic excitation function, we show the maximum and minimum values that could be obtained by changing independently the alignment of each of the two partners at each energy. These were calculated by scanning all of the possible values of  $\beta_1$  and  $\beta_2$  in eqn (13). It should be emphasised that the values of  $\beta_1$  and  $\beta_2$  that maximise/minimise the cross sections vary with the  $E_{\text{coll}}$ , especially around the resonances.

The isotropic excitation function at very low  $E_{\text{coll}}$  is found to decrease with increasing energy, a behaviour that is predicted by the Wigner threshold laws ( $\sigma \propto E_{\text{coll}}^{-1/2}$ ).<sup>63</sup> A specific preparation of the internuclear axes of the two  $D_2$  molecules makes it possible to enhance/suppress the cross sections at these low energies. As we will see below, this is unexpected as integral cross sections cannot be modified by the alignment of just one of the reactants in the limit of zero  $E_{\text{coll}}$ .<sup>67</sup> At higher  $E_{\text{coll}}$  the most salient feature of the excitation function is the presence of sharp peaks around 2.0, 2.9 and 8.9 K, the first two associated to a  $\ell = 4$  shape resonance, and the latter to a  $\ell = 5$  resonance. It is around these resonances where the cross sections could be controlled to a considerable extent.

Some of the PPs that are responsible for the stereodynamical control are shown in panel (b) of Fig. 1 as a function of  $E_{\text{coll}}$ . Only the PPs with even  $k_A$  and  $k_B$  are shown since the corresponding extrinsic  $a_0^{(k_{AB})}$  are different from zero only for even values for the simulated experiment (alignment). In the present notation, 1 corresponds to the  $D_2(v = 0, j = 2)$ , whose internal state is not modified during the collision, and 2 corresponds to the  $D_2(v = 2, j = 2)$  which is rotationally relaxed. The respective PPs are denoted as  $s_{0,0}^{(k_1, k_2)}$ . It should be stressed that if one of the two ranks  $k$  of the moment is zero, this moment will be the same as that obtained for the corresponding 3-vector correlation. The physical meaning of the PPs represented here is:

- Positive (negative) values of  $s_{0,0}^{(2,0)}$  indicate that quenching of  $D_2(v = 2, j = 2)$  is promoted when the internuclear axis of  $D_2(v = 0, j = 2)$  is aligned perpendicular (parallel) to  $\mathbf{k}$ , and hence increase the cross section for  $\beta_1 \sim 90^\circ$  ( $\beta_1 \sim 0^\circ$ ).



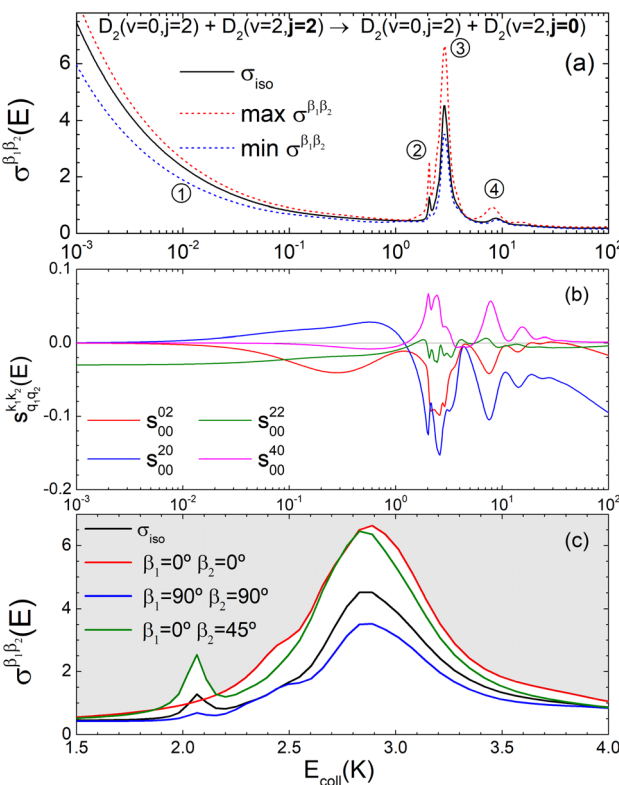


**Fig. 1** Panel (a) shows the isotropic cross section (solid black line) as a function of  $E_{\text{coll}}$  for  $D_2(v=0, j=2) + D_2(v=2, j=2) \rightarrow D_2(v=0, j=2) + D_2(v=2, j=0)$  collisions along with the maximum (red dashed line) and minimum (blue dashed line) values of the cross sections that can be achieved by a given alignment of the internuclear axes of the two diatoms. The labels 1–4 indicate the values of  $E_{\text{coll}}$  at which the dependence on  $\sigma^{\beta_1\beta_2}$  is shown in Fig. 3. Panel (b) shows the relevant polarization parameters,  $s_{q_1q_2}^{k_1k_2}$ , as functions of  $E_{\text{coll}}$ . Panel (c) shows the ICS  $\sigma^{\beta_1\beta_2}$  as functions of  $E_{\text{coll}}$  for four different preparations. The region above the maximum value of the cross section that could be achieved is shaded in grey.

- Positive (negative) values of  $s_{0,0}^{(4,0)}$  indicate that quenching of  $D_2(v=2, j=2)$  is promoted when the internuclear axis of  $D_2(v=0, j=2)$  is aligned perpendicular or parallel (tilted) to  $\mathbf{k}$ , and hence increase the cross section for  $\beta_1 \sim 90^\circ$  or  $\sim 0^\circ$  ( $\beta_1 \sim 45^\circ$ ).
- Positive (negative) values of  $s_{0,0}^{(0,2)}$  indicate that quenching of  $D_2(v=2, j=2)$  is promoted when its internuclear axis is aligned perpendicular (parallel) to  $\mathbf{k}$ , and hence increase the cross section for  $\beta_2 \sim 90^\circ$  ( $\beta_2 \sim 0^\circ$ ).
- Positive values of  $s_{0,0}^{(2,2)}$  indicate that quenching of  $D_2(v=2, j=2)$  is promoted especially when the internuclear axis of both  $D_2$  molecules is aligned parallel to  $\mathbf{k}$  and to a lesser extent when both are aligned perpendicular to  $\mathbf{k}$ , and hence increase the cross section especially for  $\beta_1 \sim 0^\circ$  and  $\beta_2 \sim 0^\circ$ . Negative values of  $s_{0,0}^{(2,2)}$  indicate that the quenching is promoted when one internuclear axis is aligned parallel to the initial relative velocity  $\mathbf{k}$  whilst the other is perpendicular to  $\mathbf{k}$  (i.e. either for  $\beta_1 \sim 0^\circ$  and  $\beta_2 \sim 90^\circ$  or for  $\beta_1 \sim 90^\circ$  and  $\beta_2 \sim 0^\circ$ ).

According to Fig. 1(b), at low  $E_{\text{coll}}$  the only relevant PP is  $s_{0,0}^{(2,2)}$  which indicates that cross sections will be enhanced when the two internuclear axes are

perpendicular to each other. With increasing  $E_{\text{coll}}$ ,  $s_{0,0}^{(2,0)}$  and  $s_{0,0}^{(0,2)}$  are also relevant, the former being positive and the latter negative, which favors the preference for collisions where the two internuclear axes are perpendicular to each other. Around the energies of the resonances the values of the PPs start oscillating and take larger absolute values, indicating the different collision mechanism at the resonance. Interestingly, for  $E_{\text{coll}}$  above 20 K, the only relevant PP is  $s_{0,0}^{(2,0)}$ , which indicates that  $D_2(v = 2, j = 2)$  quenching only depends on the alignment of the  $D_2(v = 0, j = 2)$  internuclear axis, favoring a parallel alignment with  $\mathbf{k}$ .

Panel (c) of Fig. 1 shows the excitation functions for different combinations of  $\beta_1$  and  $\beta_2$  around the energy of the  $\ell = 4$  resonance, with the shaded region representing the cross sections above the maximum values that could be achieved by any preparation. In the vicinity of the resonance, collisions in which both internuclear axes are perpendicular to  $\mathbf{k}$  minimise the cross section, while collisions for which  $D_2(v = 0, j = 2)$  is aligned parallel to  $\mathbf{k}$  and where  $D_2(v = 2, j = 2)$  is aligned either parallel or tilted to  $\mathbf{k}$  significantly enhances the cross section.

To appreciate the different extent of control that can be achieved by aligning both  $D_2$  molecules compared to that obtained when only one of the molecules is aligned, in Fig. 2 we show the isotropic excitation function along with the maximum value that can be obtained by aligning just one of the molecules, and the maximum value obtained when both molecules are aligned. Our results show that for  $E_{\text{coll}} > 2.0$  K higher cross sections can be obtained by aligning  $D_2(v = 0, j = 2)$  rather than  $D_2(v = 2, j = 2)$ . Only around the  $\ell = 5$  resonance ( $E_{\text{coll}} \sim 8$  K) there

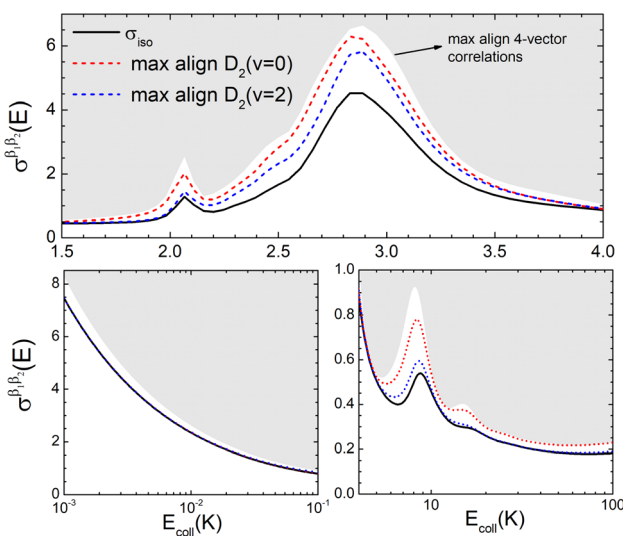


**Fig. 2** Isotropic cross section (solid black line) as a function of  $E_{\text{coll}}$  for  $D_2(v = 0, j = 2) + D_2(v = 2, j = 2) \rightarrow D_2(v = 0, j = 2) + D_2(v = 2, j = 0)$  collisions. The region above the maximum value of the cross sections that can be achieved by a given alignment of the internuclear axes of the two diatoms is shaded in grey, while the maximum cross sections that could be obtained by alignment of either  $D_2(v = 0, j = 2)$  or  $D_2(v = 2, j = 2)$  are shown as a red and blue dashed lines, respectively. Top panel shows the region around the resonance. The bottom-left panel shows the low energy region, while the bottom-right panel displays the 4–10 K energy range in logarithmic scale.



is a clear gain in the degree of control achieved by aligning both molecules, and from 20 K, the alignment of  $D_2(v = 2, j = 2)$  has almost no effect on the ICS.

The behaviour at very low energies deserves a separate analysis. As demonstrated in ref. 67, it is not possible to modify the ICS at energies where only  $\ell = 0$  contributes by the polarization of just one of the molecules (*i.e.* three-vector correlations). Mathematically, it means that the only polarization parameter,  $u_0^{(k)}$ , that is different from zero is  $u_0^{(0)}$ . It does not mean that  $\ell = 0$  scattering is insensitive to an anisotropic preparation of the reactants, and indeed in the zero energy limit the DCS depends on the alignment,<sup>39,67</sup> but simply these differences cancel out upon integration over the scattering angle. For the simpler case of an atom + diatom scattering, if  $\ell = 0, J = j$  and eqn (12) reduces to

$$u_0^{(k)} = \frac{\pi}{k^2} \sum_{m,m'} \left| S_{m',m}^{J=j} \right|^2 \langle jm, k0 | jm \rangle. \quad (15)$$

Irrespective of  $j$  and  $k$ , it is true that  $\sum_m \langle jm, k0 | jm \rangle = 0$ , so  $u_0^{(k)}$  can only be zero if  $\sum_m \left| S_{m',m}^{J=j} \right|^2$  is independent of  $m$ . This behaviour could be generalized to diatom + diatom scattering and, in fact, it is systematically observed that there is no control of ICS for  $E_{\text{coll}} \rightarrow 0$  when only one of the diatomic molecules is polarized.<sup>31,37</sup> In the case of the alignment of two molecules the situation is different. On the one hand, in eqn (12) we have two different Clebsch–Gordan coefficients, and since  $\sum_m |\langle jm, k0 | jm \rangle|^2 \neq 0$ , even if all the elements of the  $S$  matrix had the same values, the  $u_{0,0}^{(k_A, k_B)}$  would be different from zero, which opens the possibility of control over the ICS. On the other hand, at least at 1 mK, we still observe differences in the values of the  $S$  matrix even though all three vector correlations are zero for  $E_{\text{coll}} < 10$  mK. In fact, the value (and even the sign) of the  $s_{0,0}^{(2,2)}$  at  $E_{\text{coll}} = 1$  mK is different for the three systems studied.

To exemplify the extent of control attainable through the alignment of the two diatoms, we will examine four different  $E_{\text{coll}}$  values and demonstrate how changing  $\beta_1$  and  $\beta_2$  affects the cross section. These results are represented in Fig. 3 as contour maps where  $\beta_1$  is the angle that defines the direction of the internuclear axis  $D_2(v = 0, j = 2)$ , and  $\beta_2$  corresponds to the direction of  $D_2(v = 2, j = 2)$ . The color scale is shown in the side panels with red and yellow denoting values above that of the isotropic cross section, while blue indicates  $(\beta_1, \beta_2)$  regions for which the cross section is smaller. The value of the isotropic cross section is highlighted with dashed curves. To gain further insights into the collision mechanism, we combine this information with sketches of the probability density functions corresponding to the angles that maximise the cross section.

At  $E_{\text{coll}} = 10$  mK, within the cold regime, the contour map is symmetric with respect to the diagonal, which indicates that alignment of either partner yields equivalent results for the same alignment angle. The minimum value of the cross section corresponds to  $(\beta_1 = 0^\circ, \beta_2 = 0^\circ)$ , while the maximum value is attained for  $(\beta_1 = 0^\circ, \beta_2 = 90^\circ)$  or  $(\beta_1 = 90^\circ, \beta_2 = 0^\circ)$ , as expected for a collision dominated by the negative  $s_{0,0}^{(2,2)}$  moment. The cross section for  $(\beta_1 = 90^\circ, \beta_2 = 90^\circ)$  is similar to the isotropic cross section. The sketch for the alignment that maximizes the cross



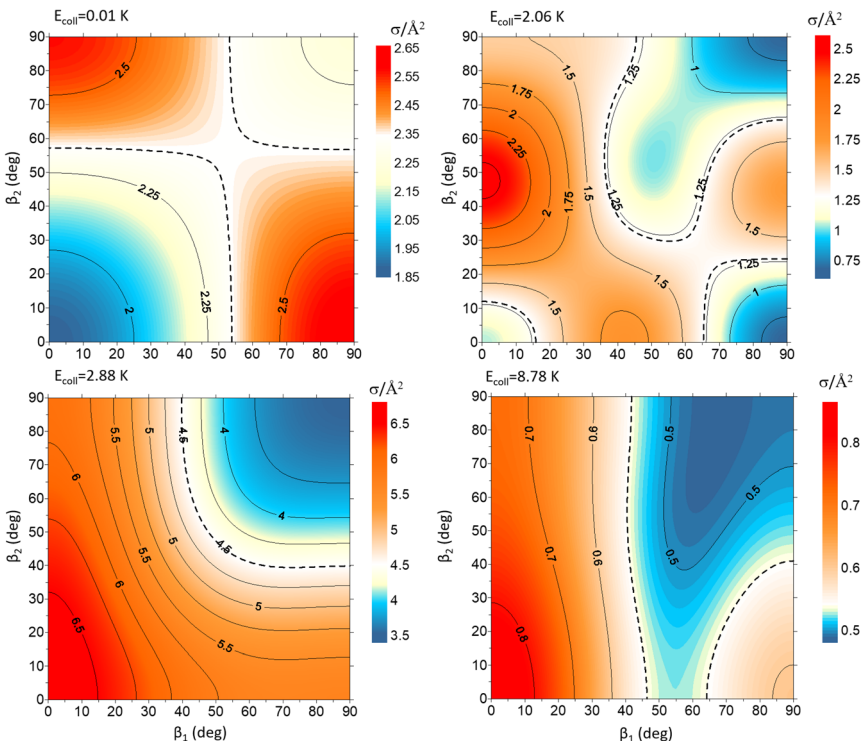


**Fig. 3** Contour maps showing the ICS  $\sigma^{\beta_1, \beta_2}$  for  $D_2(v=0, j=2) + D_2(v=2, j=2) \rightarrow D_2(v=0, j=2) + D_2(v=2, j=0)$  collisions as a function of  $\beta_1$  and  $\beta_2$  for each of the four values of  $E_{\text{coll}}$  indicated in Fig. 1.  $\beta_1$  is the angle that defines the direction of the internuclear axis of the  $D_2(v=0, j=2)$ , whose internal state does not change in the collision, whereas  $\beta_2$  refers to the  $D_2(v=2, j=2)$  molecule that experiences the quenching of its rotational level.

section is represented in Fig. 4. Please note that we do not have information about the impact parameter,  $b$ , and in this sketch we have assumed a small  $b$ , as  $\ell = 0$  dominates at this  $E_{\text{coll}}$  ( $b$  is represented in the figure as the horizontal separation between the blue and red portraits). It should be borne in mind that the direction of  $D_2(v=0, j=2)$  internuclear axis has a significant influence in the cross section, even though this molecule does not change its rovibrational state in the collision.

The plot for  $E_{\text{coll}} = 2.06$  K corresponds to the energy at which the first resonance peak is observed (see Fig. 1). The contour map is no longer symmetric, and the maximum value is obtained for  $(\beta_1 = 45^\circ, \beta_2 = 0^\circ)$ , whose sketch is represented in Fig. 4, where we have assumed a large impact parameter compatible with  $\ell = 4$  ( $b = 10.9$  Å), the partial wave associated to the resonance. There are two minima corresponding to  $(\beta_1 = 90^\circ, \beta_2 = 0^\circ, 90^\circ)$ . It is also worth noting that, in this case, the cross section could only be decreased to a small extent. Similar behaviour is observed at the two higher  $E_{\text{coll}}$  considered.

The PPs were found to vary around the  $E_{\text{coll}}$  of the resonance, and at  $E_{\text{coll}} = 2.88$  K, where the sharpest resonance peak was observed, the relative orientation that maximises the cross section is  $(\beta_1 = 0^\circ, \beta_2 = 0^\circ)$ , and in this case the contour map is again symmetric along the diagonal. The sketch of this relative polarisation is



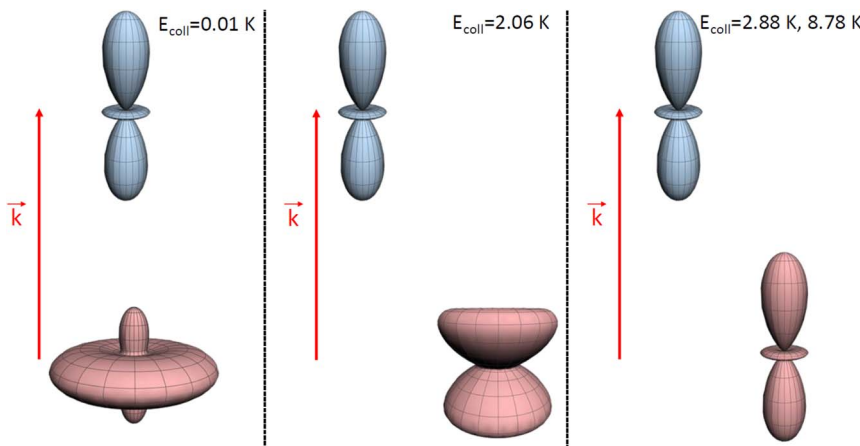


Fig. 4 Pictorial representation of the extrinsic stereodynamical portraits (distributions that graphically represent the dependence of the reaction dynamics on directions in space) showing the asymptotic spatial distributions of internuclear axes of the two partners which maximise the cross sections in  $D_2(v = 0, j = 2) + D_2(v = 2, j = 2) \rightarrow D_2(v = 0, j = 2) + D_2(v = 2, j = 0)$  collisions at the  $E_{\text{coll}}$  values indicated in Fig. 1. The portraits for  $D_2(v = 0, j = 2)$  are shown in blue while those for the  $D_2(v = 2, j = 2)$  collision partner are shown in red. In each case, the horizontal separation between the center-of-mass of the blue and red portraits qualitatively represents the value of the classical impact corresponding to the partial wave associated to the resonance that dominates scattering at each energy.

also displayed in Fig. 4, showing a preference for head-on collisions. The smallest values of the cross sections are obtained for  $(\beta_1 = 90^\circ, \beta_2 = 90^\circ)$ . Finally,  $E_{\text{coll}} = 8.78$  K corresponds to the  $\ell = 5$  resonance, and at this energy the orientation that maximises the cross sections is again  $\beta_1 = 0^\circ, \beta_2 = 0^\circ$ , while  $\beta_1 = 70^\circ, \beta_2 = 70\text{--}90^\circ$  yields the smallest cross sections.

### 3.2 $D_2(v = 0, j = 2) + D_2(v = 2, j = 2) \rightarrow D_2(v = 0, j = 0) + D_2(v = 2, j = 0)$

Now we examine the effect of the alignment of the two diatomic molecules in a process where both molecules are relaxed to their rotational ground state,  $D_2(v = 0, j = 2) + D_2(v = 2, j = 2) \rightarrow D_2(v = 0, j = 0) + D_2(v = 2, j = 0)$ . The excitation functions presented in panel (a) of Fig. 5 are qualitatively similar to those obtained when only one partner is quenched to  $j = 0$  (Fig. 1). They feature two resonances, one associated with  $\ell = 4$  at 2.83 K, and another corresponding to  $\ell = 5$  at 8.78 K. Quantitatively, the cross sections are significantly smaller, as expected for a double quenching process. Experimental detection of this channel would be hampered by the small value of the cross sections, particularly since  $D_2(v = 2, j = 0)$  is generated through single-relaxation processes with significantly higher cross-sections. To detect this channel, a method would be required that is highly sensitive to the recoil velocity and can distinguish between the  $D_2(v = 2, j = 0)$  produced by single and double quenching. The latter will imply a lower recoil energy in the center of mass equivalent to two rotational quanta. Despite this, the study of the double-quenching process illustrates the degree of control attainable through the alignment of the two diatomic molecules. In the present case, it exceeds significantly that of the single quenching process, resulting in an increase of up to a factor of three in the cross section around the resonances (a factor of 4

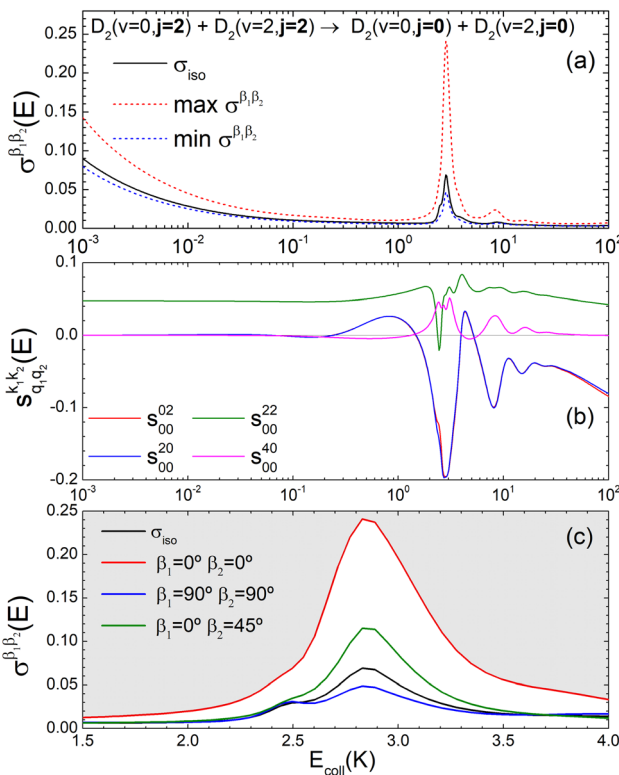


Fig. 5 (a) Isotropic cross section (solid black curve) as a function of  $E_{\text{coll}}$  for  $\text{D}_2(v=0, j=2) + \text{D}_2(v=2, j=2) \rightarrow \text{D}_2(v=0, j=0) + \text{D}_2(v=2, j=0)$  collisions. The maximum and minimum values of the cross sections that could be achieved by a given alignment of the two internuclear axes of the diatoms are shown as red and blue dashed curves, respectively. (b) The relevant  $s_{q_1 q_2}^{k_1 k_2}$  as a function of  $E_{\text{coll}}$ . (c)  $\sigma^{\beta_1 \beta_2}$  calculated as a function of  $E_{\text{coll}}$  for the four given preparations. The region above the maximum value of the cross section that could be achieved is shaded in grey.

at 3.07 K), and an increase by a factor of two at the highest energies. At the lowest energies the increase is only 50%.

Panel (b) of Fig. 5 shows the PPs responsible for the stereodynamical control. Strikingly, we observe that  $s_{0,0}^{(k_1, k_2)} \sim s_{0,0}^{(k_2, k_1)}$ , and there are only very subtle differences between  $s_{0,0}^{(2,0)} \sim s_{0,0}^{(0,2)}$  around 2 K and from 40 K. This suggests that in this process, the collision mechanism does not differentiate between the alignment of either partner, which evinces the spectator role of the vibrational quantum number at these  $E_{\text{coll}}$ . At very low  $E_{\text{coll}}$ , the value of  $s_{0,0}^{(2,2)}$  is positive and significantly different from zero. This contrasts with the results obtained for the single relaxation process, where  $s_{0,0}^{(2,2)}$  was negative at low energies. Hence, at low  $E_{\text{coll}}$  the collision prefers preparations in which both internuclear axes are aligned parallel to  $\mathbf{k}$ , *i.e.*, corresponding to a ( $\beta_1 = 0^\circ, \beta_2 = 0^\circ$ ) conformation. The  $s_{0,0}^{(2,2)}$  remains nearly constant with  $E_{\text{coll}}$ . This together with the  $s_{0,0}^{(2,0)} \sim s_{0,0}^{(0,2)}$  values, causes the arrangement ( $\beta_1 = 0^\circ, \beta_2 = 0^\circ$ ) to maximize the cross section for the whole  $E_{\text{coll}}$  range.

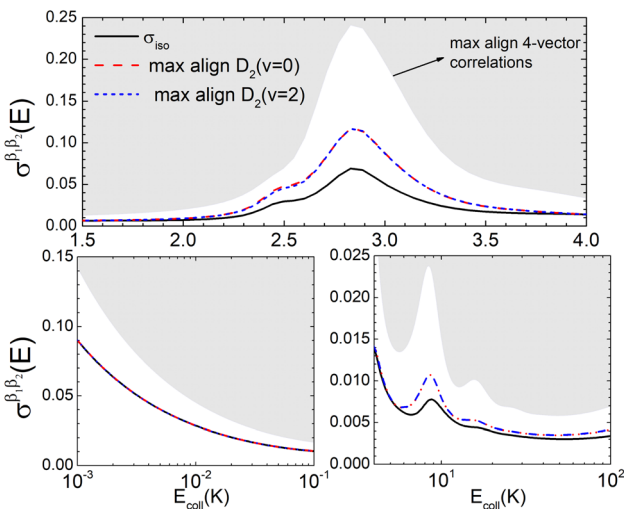


Fig. 6 Same as Fig. 2 but for  $D_2(v=0, j=2) + D_2(v=2, j=2) \rightarrow D_2(v=0, j=0) + D_2(v=2, j=0)$  collisions.

Panel (c) of Fig. 5 shows that the alignment of both partners leads to a substantial increase of the cross sections in the vicinity of the  $\ell = 4$  resonance. In this case, there is only one resonance peak, and the cross section is significantly enhanced by a  $(\beta_1 = 0^\circ, \beta_2 = 0^\circ)$  alignment.  $(\beta_1 = 0^\circ, \beta_2 = 45^\circ)$  and  $(\beta_1 = 45^\circ, \beta_2 = 0^\circ)$  lead to a small increase in the cross section. The  $(\beta_1 = 90^\circ, \beta_2 = 90^\circ)$  alignment makes the cross section smaller than the isotropic one, implying that side-on collisions are less effective in double quenching processes.

Fig. 6 illustrates that the simultaneous alignment of both internuclear axes leads to cross sections that significantly exceed (on a relative basis compared to isotropic collisions) that obtained by the alignment of just one of the molecules in the whole  $E_{\text{coll}}$  range considered here. In fact, by polarizing only one of the diatomic molecules, significant control is only achieved at the resonances, and even then, optimal alignment never results in more than an increase of 70% with respect to the isotropic cross section.

### 3.3 $D_2(v=2, j=2) + D_2(v=2, j=2) \rightarrow D_2(v=2, j=2) + D_2(v=2, j=0)$

The third case that we will examine is that in which two identical molecules collide, a  $D_2(v=2, j=2) + D_2(v=2, j=2) \rightarrow D_2(v=2, j=2) + D_2(v=2, j=0)$  collision, which corresponds to that studied experimentally by Zhou *et al.*,<sup>30</sup> and analyzed in ref. 41 under experimental conditions (same alignment for the two partners).

In contrast to the previous cases, in this system the two molecules are truly indistinguishable, and accordingly we find that  $S_{j_{AB}m'_A, m'_B j_{AB} m_A m_B}^{j,+}$  differs significantly from  $S_{j_{AB} m'_A, m'_B j_{AB} m_A m_B}^{j,-}$ , which makes impossible to discriminate the molecule that is relaxed to  $j = 0$ . Bearing that in mind, it makes no sense to attribute  $\beta_1$  and  $\beta_2$  to the alignment of one or the other partner, and although we will keep this notation,  $\beta_1$  and  $\beta_2$  are equivalent for this process.

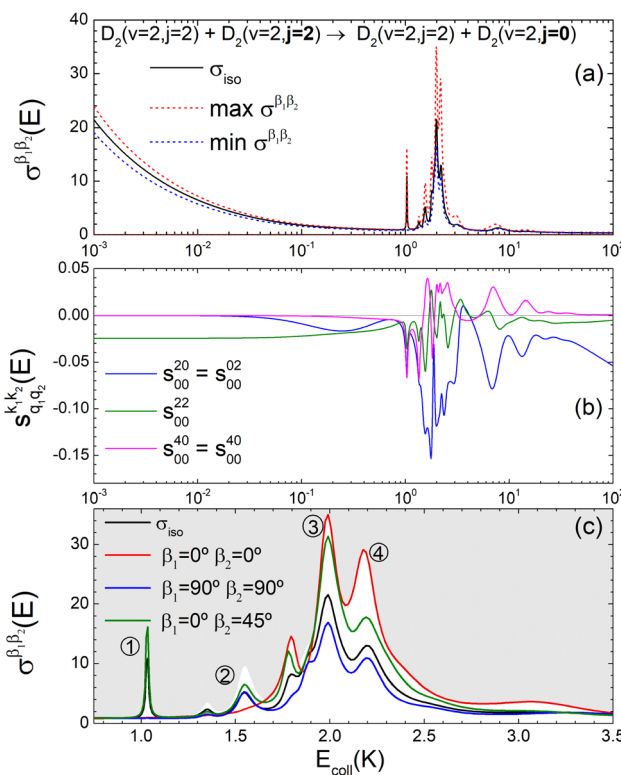
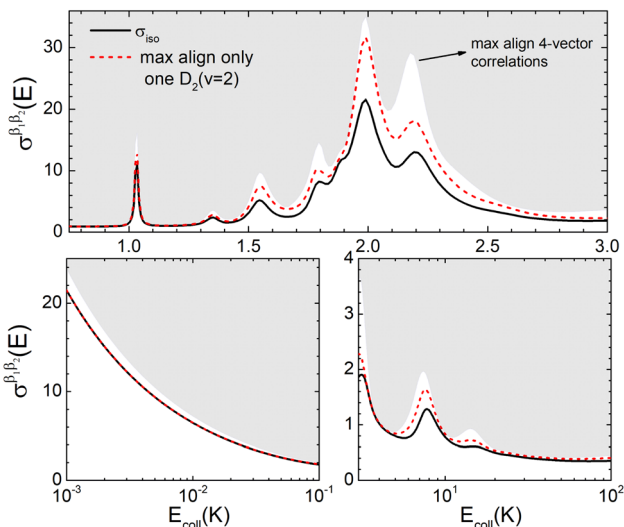


Fig. 7 (a) Isotropic cross section (solid black curve) as a function of  $E_{\text{coll}}$  for  $\text{D}_2(v=2, j=2) + \text{D}_2(v=2, j=2) \rightarrow \text{D}_2(v=2, j=2) + \text{D}_2(v=2, j=0)$  collisions. The maximum and minimum values of the cross sections that could be achieved by a given alignment of the two internuclear axes of the diatoms are shown as red and blue dashed curves, respectively. (b) The relevant polarization parameters,  $s_{q_1q_2}^{k_1k_2}(E)$ , are shown as a function of  $E_{\text{coll}}$ . (c)  $\sigma^{\beta_1\beta_2}$  calculated as a function of  $E_{\text{coll}}$  for three given preparations. The region above the maximum value of the cross section that could be achieved is shaded in grey. The labels 1–4 indicate the  $E_{\text{coll}}$  at which the dependence on  $\sigma^{\beta_1\beta_2}$  is displayed in Fig. 9.

The isotropic excitation function for this process, displayed in panel (a) of Fig. 7, exhibits features similar to those of the previous processes, but differs in the splitting of the  $\ell = 4$  resonance into six peaks, with the first three peaks also showing a significant contribution from  $\ell = 2$ . The level of control that could be attainable *via* alignment of the two molecules is somewhat smaller to that obtained for the single quenching process of  $\text{D}_2(v=0, j=2) + \text{D}_2(v=2, j=2)$ , and is very modest compared to that obtained for the double quenching process. Only in the vicinity of the resonances is the level of control significant and, as shown in Fig. 8, only for some of the peaks do their magnitudes differ significantly from those obtained by the alignment of just one of the molecules, especially for the  $E_{\text{coll}} = 2.19$  K peak.

The PPs displayed in panel (b) of Fig. 7 are qualitatively similar to those obtained for the single quenching of  $\text{D}_2(v=0, j=2) + \text{D}_2(v=2, j=2)$ , although their absolute values are slightly smaller, resulting in a lower degree of control. We attribute this to the indistinguishability of the two partners because the absolute



**Fig. 8** Isotropic cross section (solid black curve) as a function of  $E_{\text{coll}}$  for  $D_2(v=2, j=2) + D_2(v=2, j=2) \rightarrow D_2(v=2, j=2) + D_2(v=2, j=0)$  collisions. The region above the maximum value of the cross sections that could be achieved by a given alignment of one of the two  $D_2$  molecules is shown as a dashed red curve. Top panel shows the region around the resonance in a linear scale while the bottom panels show the low energy, and 3–10 K region in a logarithm  $E_{\text{coll}}$  scale.

value of  $s_{q_1 q_2}^{(k_1 k_2),+}$  is different from that of the  $s_{q_1 q_2}^{(k_1 k_2),-}$ , the former prevailing at the lowest  $E_{\text{coll}}$  due to the higher cross section associated with the + exchange parity symmetry.

To assess the extent of control attainable in the vicinity of the  $\ell = 4$  resonance, panel (c) of Fig. 7 shows the cross sections calculated at four different preparations  $(\beta_1 = 0^\circ, \beta_2 = 0^\circ)$ ,  $(\beta_1 = 90^\circ, \beta_2 = 90^\circ)$ , and  $(\beta_1 = 0^\circ, \beta_2 = 45^\circ) \equiv (\beta_1 = 45^\circ, \beta_2 = 0^\circ)$ . The combination of two partial waves ( $\ell = 2$ , and  $\ell = 4$ , the latter being dominant) alongside two exchange symmetry parities enriches the stereodynamics at the resonance. For example,  $(\beta_1 = 0^\circ, \beta_2 = 0^\circ)$  alignment leads to the highest cross sections at the two dominant peaks at 1.99 K and 2.19 K, while it leads to the vanishing of the resonance peaks at 1.03 and 1.55 K. Interestingly, the 1.03 K peak also vanishes for the apparently opposite  $(\beta_1 = 90^\circ, \beta_2 = 90^\circ)$  alignment. However, the  $(\beta_1 = 0^\circ, \beta_2 = 45^\circ)$  alignment is capable of enhancing this resonance and almost maximises the cross sections at 1.99 K.

Fig. 9 shows how changing  $\beta_1$  and  $\beta_2$  affects the cross section at some of the resonance peaks. For the  $E_{\text{coll}} = 1.03$  K peak, the contour map is very symmetrical. Interestingly, this symmetry is missing if we restrict the results for either  $\ell = 2$  or  $\ell = 4$ , the former showing a maximum for  $(\beta_1 = 0^\circ, \beta_2 = 90^\circ)$ . In fact, the cross sections for the different preparations are not only determined by  $\ell = 2, 4$  or their incoherent sum, but also for their interference (due to the distinguishability of the two  $D_2$  partners). At  $E_{\text{coll}} = 1.55$  K, the preparation  $(\beta_1 = 0^\circ, \beta_2 = 0^\circ)$  minimises the cross section, which also shrinks for  $(\beta_1 = 60^\circ, \beta_2 = 90^\circ)$  alignment. The cross section is maximised for  $(\beta_1 = 90^\circ, \beta_2 = 0^\circ)$ . Also at this energy, the cross section for a specific alignment is given by the interference between the

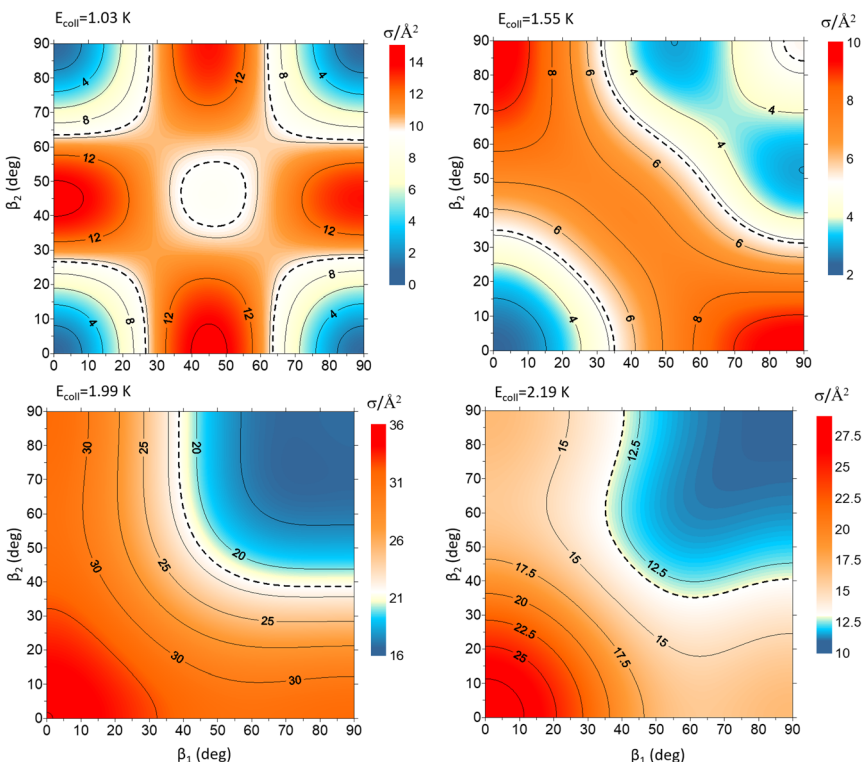


Fig. 9 Contour maps showing the  $\sigma^{\beta_1\beta_2}$  for  $D_2(v=2, j=2) + D_2(v=2, j=2) \rightarrow D_2(v=2, j=2) + D_2(v=2, j=0)$  collisions as a function of  $\beta_1$  and  $\beta_2$  for each of the four  $E_{\text{coll}}$  highlighted in Fig. 7. Since both  $D_2$  molecules are indistinguishable  $\beta_1$  and  $\beta_2$  represent the angles that define the direction of the internuclear axis of any of the two diatoms.

$\ell = 2$  and the  $\ell = 4$  contributions. At the two main resonance peaks,  $E_{\text{coll}} = 1.99$  K, and 2.19 K, it is the ( $\beta_1 = 0^\circ$ ,  $\beta_2 = 0^\circ$ ) alignment that boosts the cross section, whereas the ( $\beta_1 = 90^\circ$ ,  $\beta_2 = 90^\circ$ ) alignment suppresses it.

## 4 Conclusions

In this work we have investigated how the integral cross section of inelastic diatom-diatom collisions can be controlled by simultaneously changing the direction of the rotational angular momentum (and hence of the internuclear axis) of both diatoms. This requires the evaluation of the correlations between the following 4 vectors: the initial ( $\mathbf{k}$ ) and final ( $\mathbf{k}'$ ) relative velocities of the collision partners, and the directions of the angular momentum of the two molecules,  $\mathbf{j}_A$  and  $\mathbf{j}_B$ . The underlying quantum theory is presented in full-dimensions. As a case study, we have performed time-independent quantum scattering calculations for the rotational quenching of  $D_2(v, j=2) + D_2(v, j=2)$  collisions for three different scenarios: (a)  $v = 0 + v = 2$ , where the  $D_2(v=2, j=2)$  molecule is quenched to ( $v=2, j=0$ ); (b)  $v = 0 + v = 2$ , where both molecules are quenched to  $j = 0$ ; (c)  $v = 2 + v = 2$ , where one of the two indistinguishable molecules is quenched to  $j = 0$ .



For all cases, the cross section can be controlled over the entire range of collision energies considered, varying from the cold regime (1 mK) to 100 K. The degree of control that can be achieved is higher in the vicinity of the resonances, and especially for the quenching of both collision partners, where a suitable preparation can significantly enhance the cross section (up to a factor of four), or decrease the cross section, sometimes leading to the disappearance of the resonance. At very low energies, the alignment of only one rotational angular momentum could not lead to control of the integral cross section, whereas simultaneous alignment of both rotational angular momenta can provide some control, due to the behaviour of the  $s_{0,0}^{(2,2)}$  moments which do not vanish in the ultracold energy regime.

At higher energies, our results show that the cross sections are typically maximised/minimised when the two internuclear axes have the same alignment. For the processes studied here, the cross section is maximised when the two molecules are aligned along the initial velocity, and is minimised when both are aligned almost perpendicular to the relative initial velocity. However, this behaviour changes in the vicinity of resonances and also for energies below 1 K, in which we have also observed cases where the cross sections are maximised when the two internuclear axes are aligned perpendicular to each other. These results can be generalised to other systems and, indeed, we expect that for chemical reactions or inelastic collisions between more complex molecules a greater degree of control could be achieved by the simultaneous alignment of two internuclear axes. We anticipate that the methods and results presented here will inform future experiments on 4-vector correlations at cold or hyperthermal energies.

## Conflicts of interest

There are no conflicts of interest to declare.

## Acknowledgements

This work is supported in part by NSF grant no. PHY-2110227 (N. B.) and by a MURI grant from Army Office of Research (grant no. W911NF-19-1-0283 to H. G. and N. B.). F. J. A. acknowledges funding by the Spanish Ministry of Science and Innovation (grant PID2021-122839NB-I00). P. G. J. acknowledges grant no. PID2020-113147GA-I00 funded by MCIN/AEI/10.13039/501100011033 (Spanish Ministry of Science and Innovation).

## References

- 1 F. Wang, J. S. Lin and K. Liu, *Science*, 2011, **331**, 900–903.
- 2 F. Wang, K. Liu and T. P. Rakitzis, *Nat. Chem.*, 2012, **4**, 636–641.
- 3 F. Wang and K. Liu, *J. Chem. Phys.*, 2016, **145**, 144305.
- 4 F. Wang and K. Liu, *J. Chem. Phys.*, 2016, **145**, 144306.
- 5 H. Pan and K. Liu, *Phys. Chem. Chem. Phys.*, 2020, **22**, 10949–10956.
- 6 H. Pan and K. Liu, *Nat. Chem.*, 2022, **14**, 545–549.
- 7 Z. Karny, R. C. Estler and R. N. Zare, *J. Chem. Phys.*, 1978, **69**, 5199.
- 8 M. G. Prisant, C. T. Rettner and R. N. Zare, *Chem. Phys. Lett.*, 1982, **88**, 271.



9 Y. Wang, J. Huang, W. Wang, T. Du, Y. Xie, Y. Ma, C. Xiao, Z. Zhang, D. H. Zhang and X. Yang, *Science*, 2023, **379**, 191–195.

10 S. A. Kandel, A. J. Alexander, Z. H. Kim, R. N. Zare, F. J. Aoiz, L. Bañares, J. F. Castillo and V. Sáez-Rábanos, *J. Chem. Phys.*, 2000, **112**, 670–685.

11 H. J. Loesch and F. Stienkemeier, *J. Chem. Phys.*, 1993, **98**, 9570–9584.

12 S. A. Lahankar, J. Zhang, K. G. McKendrick and T. K. Minton, *Nat. Chem.*, 2013, **5**, 315.

13 S. A. Lahankar, J. Zhang, T. K. Minton and K. G. McKendrick, *J. Am. Chem. Soc.*, 2014, **136**, 12371–12384.

14 P. G. Jambrina, A. Zanchet, J. Aldegunde, M. Brouard and F. J. Aoiz, *Nat. Commun.*, 2016, **7**, 13439.

15 P. G. Jambrina, A. Zanchet, M. Menéndez, V. J. Herrero and F. J. Aoiz, *Phys. Chem. Chem. Phys.*, 2019, **21**, 25389.

16 K. T. Lorenz, D. W. Chandler, J. W. Barr, W. Chen, G. L. Barnes and J. I. Cline, *Science*, 2001, **293**, 2063–2066.

17 M. Brouard, H. Chadwick, C. J. Eyles, B. Hornung, B. Nichols, F. J. Aoiz, P. G. Jambrina and S. Stolte, *J. Chem. Phys.*, 2013, **138**, 104310.

18 M. Brouard, H. Chadwick, S. Gordon, B. Hornung, B. Nichols, F. J. Aoiz and S. Stolte, *J. Phys. Chem. A*, 2015, **119**, 12404–12416.

19 J. Onvlee, S. D. S. Gordon, S. N. Vogels, T. Auth, T. Karman, B. Nichols, A. van der Avoird, G. C. Groenenboom, M. Brouard and S. Y. T. van de Meerakker, *Nat. Chem.*, 2017, **9**, 226–233.

20 T. R. Sharples, J. G. Leng, T. F. M. Luxford, K. G. McKendrick, P. G. Jambrina, F. J. Aoiz, D. W. Chandler and M. L. Costen, *Nat. Chem.*, 2018, **10**, 1148–1153.

21 C. G. Heid, I. P. Benthem, V. Walpole, P. G. Jambrina, F. J. Aoiz and M. Brouard, *J. Phys. Chem. Lett.*, 2021, **12**, 310.

22 C. G. Heid, V. Walpole, M. Brouard, P. G. Jambrina and F. J. Aoiz, *Nat. Chem.*, 2019, **11**, 662.

23 O. Ghafur, A. Rouzée, A. Gijsbertsen, W. Kiu Siu, S. Stolte and M. J. J. Vrakking, *Nat. Phys.*, 2009, **5**, 289.

24 A. Gijsbertsen, H. Linnartz, C. A. Taatjes and S. Stolte, *J. Am. Chem. Soc.*, 2006, **128**, 8777.

25 H. Zhou, W. E. Perreault, N. Mukherjee and R. N. Zare, *J. Chem. Phys.*, 2021, **154**, 104309.

26 H. Zhou, W. E. Perreault, N. Mukherjee and R. N. Zare, *Science*, 2021, **374**, 960–964.

27 W. E. Perreault, N. Mukherjee and R. N. Zare, *J. Chem. Phys.*, 2019, **150**, 174301.

28 W. E. Perreault, N. Mukherjee and R. N. Zare, *Science*, 2017, **358**, 356–359.

29 W. E. Perreault, N. Mukherjee and R. N. Zare, *Nat. Chem.*, 2018, **10**, 561–567.

30 H. Zhou, W. E. Perreault, N. Mukherjee and R. N. Zare, *Nat. Chem.*, 2022, **14**, 658–663.

31 P. G. Jambrina, J. F. E. Croft, N. Balakrishnan and F. J. Aoiz, *Phys. Chem. Chem. Phys.*, 2021, **23**, 19364.

32 M. Morita, Q. Yao, C. Xie, H. Guo and N. Balakrishnan, *Phys. Rev. Res.*, 2020, **2**, 032018(R).

33 M. Morita and N. Balakrishnan, *J. Chem. Phys.*, 2020, **153**, 184307.

34 M. Morita and N. Balakrishnan, *J. Chem. Phys.*, 2020, **153**, 091101.

35 J. F. E. Croft, N. Balakrishnan, M. Huang and H. Guo, *Phys. Rev. Lett.*, 2018, **121**, 113401.



36 J. F. E. Croft and N. Balakrishnan, *J. Chem. Phys.*, 2019, **150**, 164302.

37 P. G. Jambrina, J. F. E. Croft, H. Guo, M. Brouard, N. Balakrishnan and F. J. Aoiz, *Phys. Rev. Lett.*, 2019, **123**, 043401.

38 P. G. Jambrina, L. González-Sánchez, M. Lara, M. Menéndez and F. J. Aoiz, *Phys. Chem. Chem. Phys.*, 2020, **22**, 24943–24950.

39 P. G. Jambrina, M. Morita, J. F. E. Croft, F. J. Aoiz and N. Balakrishnan, *J. Phys. Chem. Lett.*, 2022, **13**, 4064–4072.

40 D. Yang, D. Xie and H. Guo, *J. Phys. Chem. Lett.*, 2022, **13**, 1777–1784.

41 P. G. Jambrina, J. F. E. Croft, J. Zuo, H. Guo, N. Balakrishnan and F. J. Aoiz, *Phys. Rev. Lett.*, 2023, **130**, 033002.

42 J. F. E. Croft, P. G. Jambrina, F. J. Aoiz, H. Guo and N. Balakrishnan, *J. Phys. Chem. A*, 2023, **127**, 1619–1627.

43 D. Case and D. Herschbach, *Mol. Phys.*, 1975, **30**, 1537–1564.

44 D. A. Case and D. R. Herschbach, *J. Chem. Phys.*, 1976, **64**, 4212–4222.

45 A. J. Orr-Ewing and R. N. Zare, *Annu. Rev. Phys. Chem.*, 1994, **45**, 315–366.

46 M. P. de Miranda and D. C. Clary, *J. Chem. Phys.*, 1997, **106**, 4509–4521.

47 M. P. de Miranda, F. J. Aoiz, L. Bañares and V. Saéz-Rábanos, *J. Chem. Phys.*, 1999, **111**, 5368.

48 F. J. Aoiz and M. P. de Miranda, in *Tutorials in Molecular Reaction Dynamics*, ed. M. Brouard and C. Vallance, RSC Publishing, 2010.

49 J. Aldegunde, M. P. de Miranda, J. M. Haigh, B. K. Kendrick, V. Saez-Rabanos and F. J. Aoiz, *J. Phys. Chem. A*, 2005, **109**, 6200–6217.

50 S. K. de Miranda, M. P. Pogrebnya and D. C. Clary, *Faraday Discuss.*, 1999, **113**, 119–132.

51 G. G. Balint-Kurti and O. S. Vasyutinskii, *J. Phys. Chem. A*, 2009, **113**, 14281–14290.

52 M. Costes and C. Naulin, *Chem. Sci.*, 2016, **7**, 2462.

53 A. B. Henson, S. Gersten, Y. Shagam, J. Narevicius and E. Narevicius, *Science*, 2012, **338**, 234.

54 P. Paliwal, N. Deb, D. M. Reich, A. van der Avoird, C. P. Koch and E. Narevicius, *Nat. Chem.*, 2021, **13**, 94.

55 S. D. S. Gordon and A. Osterwalder, *Int. Rev. Phys. Chem.*, 2020, **39**, 109.

56 S. Y. T. van de Meeraker, H. L. Bethlehem, N. Vanhaecke and G. Meijer, *Chem. Rev.*, 2012, **112**, 4828.

57 A. Von Zastrow, J. Onvlee, S. N. Vogels, G. C. Groenenboom, A. van der Avoird and S. Y. T. van de Meeraker, *Nat. Chem.*, 2014, **6**, 216.

58 S. N. Vogels, J. Onvlee, S. Chefdeville, A. van der Avoird, G. C. Groenenboom and S. Y. T. van de Meerakker, *Science*, 2015, **350**, 787–790.

59 V. Plomp, X. Wang, F. Lique, J. Klos, J. Onvlee and S. Y. T. van de Meeraker, *J. Phys. Chem. Lett.*, 2021, **12**, 12210.

60 R. Krems, *TwoBC – Quantum Scattering Program*, University of British Columbia, Vancouver, Canada, 2006.

61 J. Zuo, J. F. E. Croft, Q. Yao, N. Balakrishnan and H. Guo, *J. Chem. Theory Comput.*, 2021, **17**, 6747–6756.

62 W. M. Huo and S. Green, *J. Chem. Phys.*, 1996, **104**, 7572–7589.

63 J. Z. H. Zhang, *Theory and Application of Quantum Molecular Dynamics*, World Scientific, 1998.

64 K. Takayanagi, *Adv. At. Mol. Phys.*, 1965, **1**, 149–194.



65 J. Pérez-Ríos, M. Bartolomei, M. I. Campos-Martínez and R. Hernández-Lamoneda, *J. Phys. Chem. A*, 2009, **113**, 14952.

66 D. L. Johnson, R. S. Grace and J. G. Skofronick, *J. Chem. Phys.*, 1979, **71**, 4554–4569.

67 J. Aldegunde, J. M. Alvariño, M. P. de Miranda, V. Sáez-Rábanos and F. J. Aoiz, *J. Chem. Phys.*, 2006, **125**, 133104.

68 H. R. Sadeghpour, J. L. Bohn, M. J. Cavagnero, B. D. Esry, I. I. Fabrikant, J. H. Macek and A. R. P. Rau, *J. Phys. B: At., Mol. Opt. Phys.*, 2000, **33**, R93.

